Article

PANI-Based Wearable Electrochemical Sensor for pH Sweat Monitoring

Francesca Mazzara [1], Bernardo Patella [1], Chiara D'Agostino [1], Maria Giuseppina Bruno [1], Sonia Carbone [1], Francesco Lopresti [1], Giuseppe Aiello [1], Claudia Torino [2], Antonio Vilasi [2], Alan O'Riordan [3] and Rosalinda Inguanta [1,*]

[1] Applied Physical Chemistry Laboratory, Department of Engineering, Università degli Studi di Palermo, Viale delle Scienze, 90128 Palermo, Italy; francesca.mazzara04@unipa.it (F.M.); bernardo.patella@unipa.it (B.P.); chiara.dagostino95@gmail.com (C.D.); giusy1696@gmail.com (M.G.B.); carbonesonia3@gmail.com (S.C.); francesco.lopresti01@community.unipa.it (F.L.); giuseppe.aiello03@unipa.it (G.A.)

[2] Istituto di Fisiologia Clinica (IFC)-Consiglio Nazionale delle Ricerche, 89126 Reggio Calabria, Italy; ctorino@ifc.cnr.it (C.T.); avilasi@ifc.cnr.it (A.V.)

[3] Nanotechnology Group, Tyndall National Institute, University College Cork, Dyke Prade, T12 R5CP Cork, Ireland; alan.oriordan@tyndall.ie

* Correspondence: rosalinda.inguanta@unipa.it

Abstract: Nowadays, we are assisting in the exceptional growth in research relating to the development of wearable devices for sweat analysis. Sweat is a biofluid that contains useful health information and allows a non-invasive, continuous and comfortable collection. For this reason, it is an excellent biofluid for the detection of different analytes. In this work, electrochemical sensors based on polyaniline thin films deposited on the flexible substrate polyethylene terephthalate coated with indium tin oxide were studied. Polyaniline thin films were abstained by the potentiostatic deposition technique, applying a potential of +2 V vs. SCE for 90 s. To improve the sensor performance, the electronic substrate was modified with reduced graphene oxide, obtained at a constant potential of -0.8 V vs. SCE for 200 s, and then polyaniline thin films were electrodeposited on top of the as-deposited substrate. All samples were characterized by XRD, SEM, EDS, static contact angle and FT-IR/ATR analysis to correlate the physical-chemical features with the performance of the sensors. The obtained electrodes were tested as pH sensors in the range from 2 to 8, showing good behavior, with a sensitivity of 62.3 mV/pH, very close to a Nernstian response, and a reproducibility of 3.8%. Interference tests, in the presence of competing ions, aimed to verify the selectivity, were also performed. Finally, a real sweat sample was collected, and the sweat pH was quantified with both the proposed sensor and a commercial pH meter, showing an excellent concordance.

Keywords: pH sensor; sweat; polyaniline; wearable sensor; electrochemical sensor; reduced graphene oxide

1. Introduction

In recent years, wearable sensors (WS), able to test body fluids such as blood, urine, saliva, tears and sweat, have recorded a rapid diffusion, due to their low-cost technology [1–5] and the capability of continuously measuring changes in physiological parameters in real time [6–12]. For monitoring health conditions, it is possible to analyze the analytes contained in different body fluids, especially in sweat, since it is very easy to collect and allows easy measurement of biomarkers. Sweat also offers higher volumes than other body fluids and makes the placement of the sensor in different body areas possible, without impeding the natural movements [13,14]. The possibility of using non-invasive measurement systems is of extreme importance in extremely sensitive patients, such as those suffering from neurodegenerative diseases or in children [8,15]. In this perspective, electrochemical sensors appear to be very interesting because they allow carrying out

analyses in situ, are fast, reliable and inexpensive and also do not require highly specialized personnel [16–18].

A wearable electrochemical sensor benefits from the sweat produced by the eccrine glands, a colorless liquid with a variable composition depending on the part of the body considered. Eccrine sweat is clear and odorless, and it is composed of 98–99% water; it also contains NaCl, fatty acids, lactic acid, citric acid, ascorbic acid, urea and uric acid [19]. It is important to know the concentration intervals of electrolytes and metabolites contained in sweat. The deviation from the typical values allows a fast diagnosis of specific diseases. For example, concentrations outside the normal range for chloride and sodium ions become a parameter for the diagnosis of cystic fibrosis [20], and alterations in potassium ions are a symptom of decompensated diabetes mellitus and hypoaldosteronism [21], while abnormal values of uric acid are symptomatic of gout formation [22]. Another crucial parameter for the diagnosis of diseases is the sweat pH. It reflects the level of metabolism and homeostasis of the body [23], and a decompensation in its values can help to identify the onset of different diseases. Patients with type II kidney stones or diabetes have a lower pH than normal values [24], while pH variations outside the range of 4–8 are symptoms of skin disorders, such as dermatitis, ichthyosis, fungal infections and acne [25]. Furthermore, values up to pH 9 have been found in patients affected by cystic fibrosis [26] due to the defect in bicarbonate reabsorption. Moreover, as reported in [27], the monitoring of the pH during exercise can be very useful to predict the onset of metabolic alkalosis.

Different materials have been proposed to fabricate sensors for pH measurement such as iridium oxide [28], carbon [29], poly(3,4-ethylenedioxythiophene):poly(styrene sulfonate) [26], polyaniline/polyurethane [30], gold/polyaniline [31], palladium/palladium oxide [32], graphite [33] and graphite-polyurethane [34]. Polyaniline (PANI) is a very important material for the technological development of all solid-state pH sensors, and, in fact, several PANI-based electronic devices have been developed for very different applications [35]. This is the oxidative polymeric product of aniline typically carried out under acidic conditions to impart specific properties to the polymer [36,37]. PANI can exist in three different, non-conducting oxidation states: leukoemeraldine, pernigraniline and emeraldine oxidation forms. The only conductive form of PANI is the emerald salt, obtained by doping or protonation of the emeraldine base [38]. PANI thin films offer interesting electrochromic properties when subjected to an electric field that induce changes in the polymer color, from yellow to green, or to dark blue, according to reduction or oxidation [39]. Moreover, PANI showed excellent pH sensitivity when utilized in different types of PANI-based pH sensors [40]. PANI films can be obtained by different fabrication methods such as in situ chemical oxidative polymerization [41], γ-irradiation [42], spraying and drop casting [43], plasma polymerization [44], Buchwald–Hartwig polymerization [45], dip coating [46], spin coating [47] and electro-polymerization [48]. Among the different manufacturing methods, the electrochemical one appears extremely interesting because it is fast, easy to scale and simple. Furthermore, it allows obtaining different materials in different morphologies, successfully applicable and with excellent results in different electrochemical devices [49–57]. In particular, in the case of PANI, the electrodeposition method is very suitable because it permits controlling its physical-chemical characteristics [58–61].

In this work, an electrochemical pH sensor based on PANI was studied. A flexible substrate, polyethylene terephthalate coated with indium tin oxide (ITO-PET), was electrochemically covered with PANI. To improve the sensor performance, electrodes were also modified by electrochemical deposition of reduced graphene oxide (rGO). In fact, as reported in our previous works, the excellent electrocatalytic properties of rGO ensure the increase in the sensitivity of electrochemical sensors [56,62]. In particular, we developed a simple process divided into two very short stages (first stage: deposition of rGO; second stage: deposition of PANI), which allows obtaining a double-layer electrode quickly and easily. In the vast majority of the literature data, rGO/PANI electrodes are obtained with different methods (chemical, hydrothermal, in situ polymerization) that are more complicated and time-consuming and which also require numerous reagents [63–66]. The

only paper comparable to ours is that of Xue et al. [67], where, however, the electrode preparation procedure is really long and complex compared to the one proposed by us.

The electrodes were tested as pH sensors using different buffer solutions, from 2 to 8, by the open circuit potential (OCP) technique. The ITO-PET/rGO/PANi electrodes show excellent features in terms of sensitivity and reproducibility. In addition, interference tests, in the presence of competing ions typically present in sweat, were conducted. Finally, the sweat pH of a real sample was quantified with both the proposed sensor and a commercial pH meter, showing excellent results.

2. Materials and Methods

2.1. Chemicals and Apparatus

ITO/PET sheets (resistivity 60 $\Omega \cdot$cm), acetic acid, potassium dihydrogen phosphate, potassium hydroxide, trisodium citrate and sulfuric acid were purchased from Sigma Aldrich, while aqueous graphene oxide suspension (4 mg/mL) came from Graphena. Sodium acetate, aniline and potassium hydrogen phosphate were purchased from Merck, and the buffer solution came from Hanna Instruments. 2-Pure propanol, glacial acetic acid, potassium chloride, hydrochloric acid and ammonia (28% vol) were purchased from Carlo Erba reagents. All chemicals were used as received and dissolved in ultrapure water (Type 1, with a resistivity greater than 18 M$\Omega \cdot$cm).

The electrochemical fabrication and characterization were carried out by means of a PARSTAT 2273 potentiostat, employing a three-electrode cell in which the reference electrode was a saturated calomel electrode (SCE), the counter electrode was a platinum mesh and the working electrode was the PANI-based electrode.

Electrodes were characterized by X-ray diffraction (XRD) using a RIGAKU diffractometer (model: D-MAX 25,600 HK). All diffractograms were obtained in the 2θ range from 5° to 100°, with a step of 0.02° and a measuring time of 0.5 s for the step, using copper Kα radiation (λ = 1.54 Å), a tube voltage of 40 kV and a current of 60 mA. Diffraction patterns were analyzed by comparison with the literature data.

Morphology and uniformity were analyzed by scanning electron microscopy (SEM) using a FEI FEG-ESEM (model QUANTA 200) equipped with an X-ray energy-dispersive probe (EDS) that was used to evaluate the elemental composition of the samples. SEM and EDS analyses were performed on different areas of the samples in order to verify their homogeneity and uniformity.

FT-IR/ATR analysis (Perkin-Elmer FT-IR/NIR Spectrum 400 spectrophotometer) was carried out in order to investigate the chemical surface properties of the samples. Four accumulation scans with a resolution of 4 cm^{-1} were collected for each sample in the range 4000–450 cm^{-1}.

An FTA 1000 (First Ten Ångstroms, UK) instrument was used to perform the static contact angles measured by using the buffer at different pH as fluid. In particular, a droplet of solution (~4 μL) was dropped on the surface of electrodes, and the images were taken after 10 s.

2.2. Electrode Fabrication

Prior to deposition, the ITO-PET substrate was ultrasonically cleaned for 5 min in isopropanol, rinsed with ultrapure water and dried at room atmosphere for further use. An ITO-PET sheet was employed as a substrate with the aim to ensure some flexibility in the sensors. The sensors were obtained by electrodeposition of polyaniline following the procedure detailed in [68] by use of an electrolytic solution of 100 mM of aniline in 1 M of H$_2$SO$_4$. In order to deposit PANI, the potentiostatic deposition technique was employed, applying a potential of +2 V vs. SCE for 90 s, in a standard electrochemical system with three electrodes at room temperature. After the deposition, the film was gently rinsed with distilled water and dried at 50 °C for an hour.

In order to improve the performances of the electrode, a thin film of reduced graphene oxide was deposited on the ITO substrate prior to the deposition of the PANI film. [69]. In particular, 0.5 mg/mL of GO suspension was dissolved in acetate buffer solution (pH 5.4), and the deposition was carried out at a constant potential of -0.8 V vs. SCE for 200 s. The electrodeposition of PANI on this obtained substrate followed the process previously shown. The produced electrodes offered a surface area of about 0.8 cm^{-2}.

2.3. Electrochemical Detection of pH

The open circuit potential (OCP) technique was used for sensor characterization and optimization. All measurements were conducted at room temperature for a time of 250 s in order to determine the sensor response speed to reach the stationary state. The sensors were placed on buffer solutions at different pH (range between 2 and 8) to simulate the typical values of human sweat. In particular, the buffer solutions at different pH were phosphate buffer solutions (pH 6–8), acetate buffer solution (pH 4–5) and citrate buffer solution (pH 2–3). The change in the OCP value that depends on pH was measured. With the aim to evaluate the selectivity of the sensor towards H$^+$ ions, interference tests were carried out in the presence of ions commonly present in sweat such sodium, chloride, ammonium and potassium. The selectivity of the sensor was studied at pH 6 because it is very close to the average value of real human sweat samples. All experiments were carried out 3 times, and the average value of these experiments was plotted.

2.4. Sweat Collection and Testing

In order to validate the sensor, sweat was collected from a healthy subject following the method proposed in [70]. After collection, sweat was tested without any other pre-treatment. Sweat pH was measured using a HANNA pH meter (HI 2210).

3. Results and Discussion

3.1. Electrode Fabrication and Characterization

PANI was deposited on the working electrode by potentiostatic deposition in a solution of 1 M H$_2$SO$_4$, and 100 mM of aniline was added. During the electrochemical deposition (Figure 1A), after 60 s, the current density reaches a plateau at about 12 mA cm^{-2}, attaining the formation of a very homogeneous working electrode of a green color, Figure S1.

In order to verify the deposition of PANI, XRD analysis was carried out. Figure 1B shows the XRD diffraction pattern of PANI on the ITO glass substrate. The ITO glass substrate was used to avoid the very broad diffraction peak of PET that is located in the 2θ range from 20° to 30° [71], where the main diffraction peaks of PANI are also present. The peaks at 29.43°, 34.17° and 50.09°, reported in the inset, were attributed to the ITO glass substrate. The peaks located at 9.67°, 19.47° and 25.45° were attributed to PANI for comparison with the literature data [72,73]. The high intensity of PANI peaks is due to the formation of a thin polymer layer with a good crystallinity which, as reported in [72,73], indicates a good conductivity of the PANI.

Figure 1C,D show SEM analysis of the electrode at different magnifications. It is possible to notice the uniform deposition of PANI. In particular, the PANI layer is constituted of a uniform layer where nano-plates and nano-flowers, typical of PANI, can be observed [37,74].

With the aim to optimize the sensitivity of the electrode, the ITO-PET substrate was modified with rGO before PANI deposition. By doing so, a double-layer rGO/PANI electrode was obtained on the ITO/PET substrate. rGO was deposited in the potentiostatic mode using an aqueous suspension of graphene oxide.

Figure 2A shows the deposition curve of rGO on the ITO-PET surface. As observed in previous works [75,76], a steady-state current density (-150 μA cm^{-2}) is achieved after 100 s. The as-obtained substrate was then covered with PANI by electrochemical polymerization (Figure S2). At the beginning of the deposition, the growth curves show a different trend as the electrode/solution interface is different. Once the electrode surface is

completely covered with PANI (according to the growth curves, this happens after about 20–30 s), the substrate no longer influences the deposition, and, in fact, the deposition current density reaches a plateau of 11 mA cm^{-2}, showing no significant changes compared to PANI deposition on the ITO-PET surface.
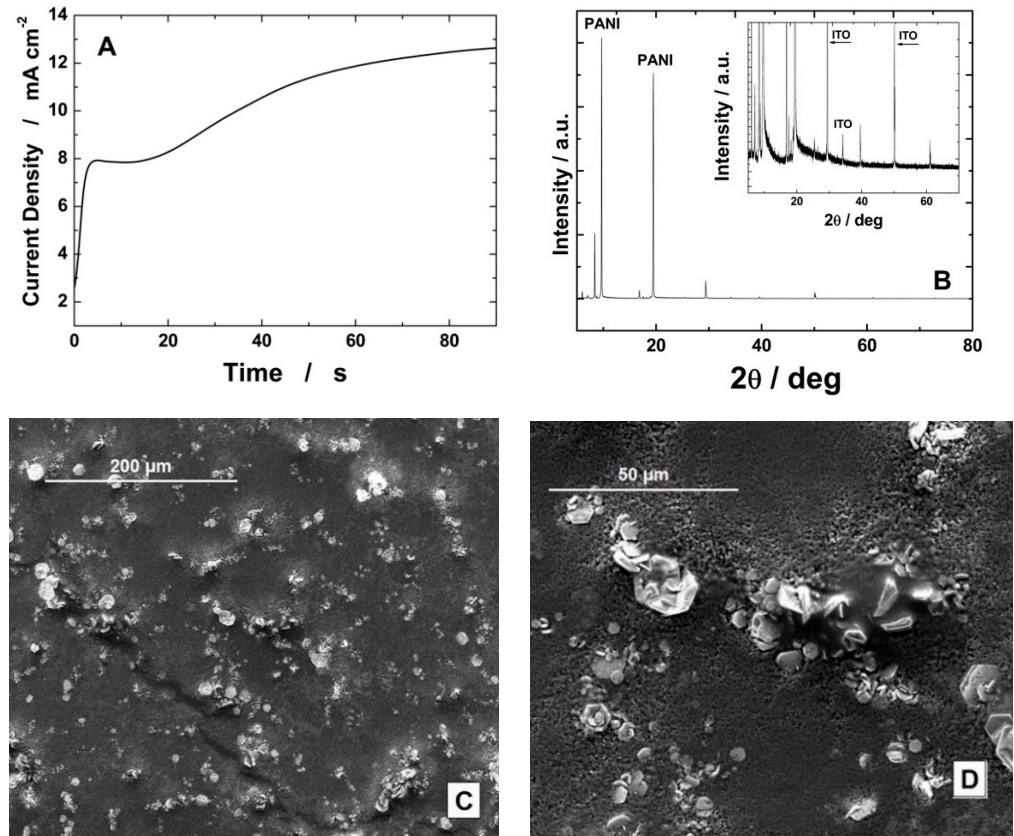

Figure 1. (**A**) Growth curve for the electrochemical deposition of PANI on ITO-PET substrate; (**B**) XRD pattern of PANI-ITO glass; (**C**,**D**) SEM images of PANI/ITO-PET electrode.
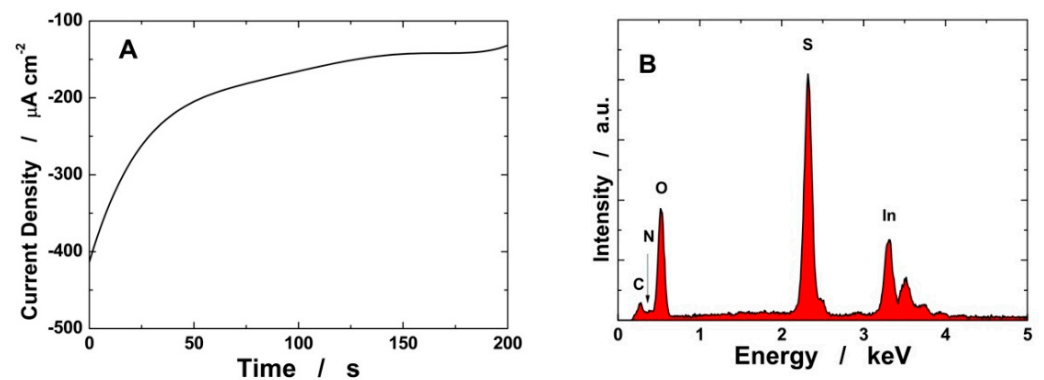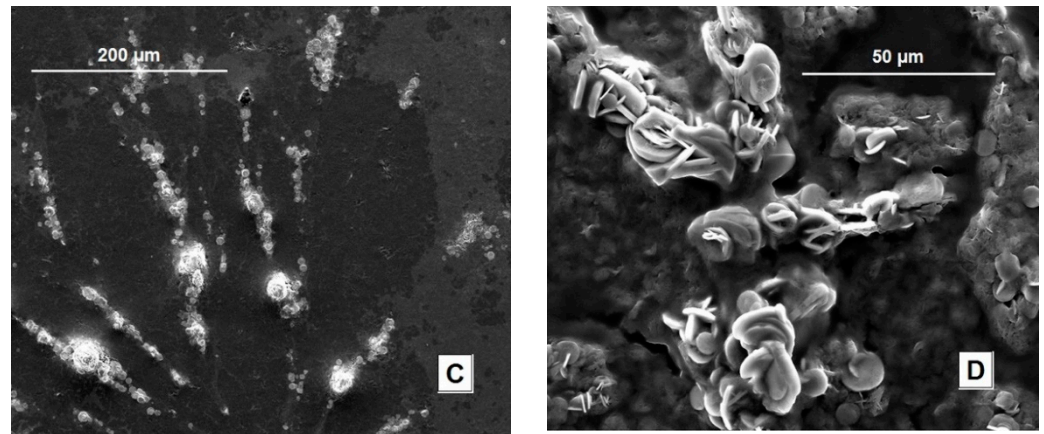

Figure 2. *Cont.*

Figure 2. (**A**) Growth curve for the electrochemical deposition of rGO on ITO-PET substrate; (**B**) EDS spectrum of PANI/rGO/ITO-PET; (**C,D**) SEM images of PANI/rGO/ITO-PET electrode.

In Figure 2B, the EDS spectrum of the PANI-rGO-ITO electrode is reported. In the spectrum, the N peak indicates the presence of PANI, while the peak of S comes from the doping of PANI by H_2SO_4. Carbon and oxygen peaks are mainly derived from the PET substrate and the electrodeposited rGO. The indium peak, overlapping the tin peak, comes from the ITO coating.

SEM analysis of the PANI/rGO/ITO-PET samples is reported in Figure 2C,D. rGO was not visible because the surface of the electrode was totally and uniformly covered with PANI, Figure 2C. Figure 2D clearly shows the formation of nano-flowers that thicken in some areas of the electrode. The SEM analysis of the samples was carried out on different points of the sample surface; we observed that the morphology shown in Figures 1 and 2 is the same in the different areas, and, consequently, it can be said that the sample is macroscopically uniform.

As reported in the literature, the PANI morphology depends on the type of acid used to prepare the deposition solution, and the flower shape is the typical form observed with H_2SO_4 [77]. In comparison to Figure 1D, the nano-flowers formed on ITO-rGO have a higher dimension, but they are less evenly distributed on the sample surface.

The electrodes were also analyzed by static contact angle measurements and FTIR-ATR. In Figure 3A, the FT-IR/ATR spectra of deposited PANI and PANI/rGO films are reported. For comparison, the spectrum of dry GO is also reported.
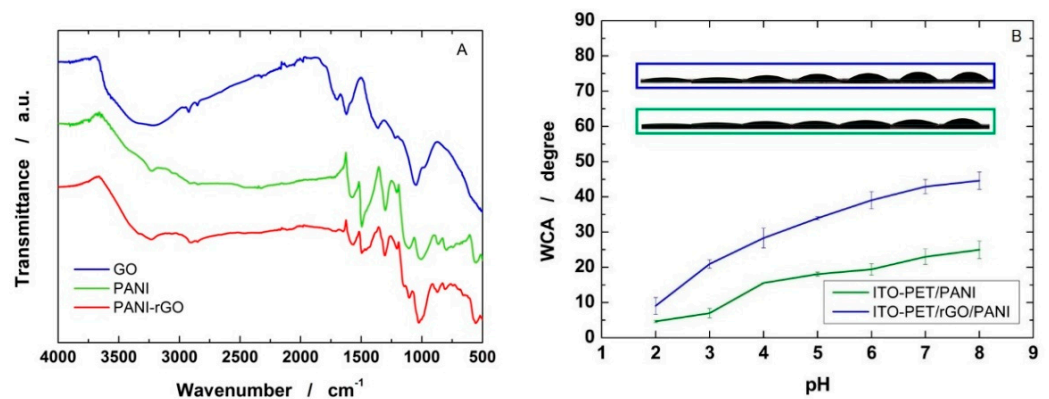

Figure 3. (**A**) FT-IR/ATR spectra of GO, PANI and PANI-rGO samples; (**B**) contact angle measurements on electrodes as a function of pH.

According to FTIR spectra, GO shows multiple bands ascribable to oxygen-derived moieties, e.g., the broad band between 2500 and 3200 cm^{-1} is from the carboxyl COOH groups forming hydrogen bonds. The characteristic peaks for carboxyl C=O were seen at 1735 cm^{-1}. The peaks at 1573 cm^{-1} and 1116 cm^{-1} are attributed to the aromatic C=C group and C-O, respectively [78].

The PANI film shows two characteristic peaks in the presence of sulfuric acids, the C=C stretching vibration of quinonoid and benzenoid rings at 1590 cm^{-1} and 1505 cm^{-1}, respectively [79]. Other peaks at 1308 cm^{-1} and 1202 cm^{-1} are attributed to C–N and C=N, respectively. Additionally, peaks at 813 and 1147 cm^{-1} are assigned to the out-of-plane deformation vibration for the 1,4 disubstituted benzene ring, γ(C–H), in the linear PANI backbone and the B–NH$^+$=Q stretching, respectively [80]. In the FTIR spectra of PANI/rGO, we can clearly see that all characteristic peaks of PANI and some typical peaks of rGO are shown. In particular, a new shoulder peak appears at 3235 cm^{-1}, which was attributed to the hydrogen bond interaction between PANI and rGO [81].

The C=C stretching vibrations of the quinonoid and benzenoid rings in PANI/rGO shift from 1590 and 1505 cm^{-1} to 1580 and 1496 cm^{-1}, respectively. The spectral red shift phenomenon confirms that PANI-rGO nanocomposites have a certain degree of conjugation due to the π–π interaction between PANI and rGO [81]. The oxygen-derived moieties typical of GO are hardly visible in the PANI/rGO systems, thus suggesting the effective reduction of GO during the deposition [78].

Figure 3B shows the contact angle (CA) measurements. As it can be observed, the CA increases with the increase in pH according to the behavior found by Blinova et al. [82]. In particular, the CA of PANI is closely related to the type of acid used for doping. The PANI doped with 1 M H$_3$PO$_4$ is more hydrophilic than PANI doped with 1 M HCl [82]. In this work, we used sulfuric acid, and we obtained lower contact angle values and, consequently, a more hydrophilic surface. As expected [83], the presence of rGO makes the electrode surface less hydrophilic, even if the contact angle values are still low and the surface can therefore be considered hydrophilic. As we will see below, the electrode with rGO, despite having a slightly lower wettability, is the one with the greatest sensitivity, indicating that the excellent electrocatalytic properties of rGO prevail over its effect on wettability.

3.2. Electrochemical Detection of pH

The electrodeposited PANI was used as a sensing material to obtain a sensitive and accurate sensor for pH. The pH values of the analyzed solution were correlated with OCP measurements conduced for a time of 250 s. By the OCP values, the pH of the solution can be calculated using Nernst's equation:

$$E = E_0 + \frac{RT}{nF} \ln a_{H^+} \tag{1}$$

E_0 is the standard redox potential, R is the universal gas constant (8.314 J K^{-1} mol^{-1}), T is the temperature ($^\circ$K), n is the number of electrons involved in the electrochemical reaction, F is the Faraday constant (96,485 C mol^{-1}) and a_{H^+} is the activity of hydrogen ions.

Figure 4 shows the obtained results using PANI/ITO-PET sensors. As it can be observed in Figure 4A, the measurement time chosen is conservative, and, indeed, the stationary state was already achieved after about 150 s. The slope of the calibration line, Figure 4B, is about 38 mV/pH, with an R^2 of 0.988. All measurements were carried out three times, and the main values are reported with the standard deviation (SD). More marked SDs were recorded for acid pH values, with the highest value of 19.7% for pH 2. The SD gradually decreased with the increase in pH, reaching a very low value for pH higher than 7. We think that this behavior is due to an instability of the ITO substrate at an extremely acidic pH [71] which can cause its partial dissolution and therefore a non-reproducible behavior.
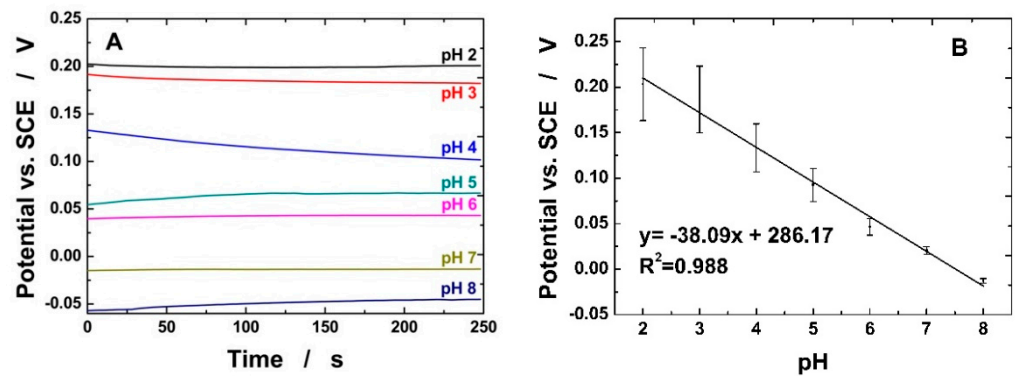
Figure 4. (**A**) OCP vs. time curves; (**B**) calibration line of PANI/ITO-PET electrode.

Figure 5A shows the OCP measurements of the PANI/rGO/ITO-PET electrode. In comparison to PANI/ITO-PET, better results were obtained both in terms of the response time and reproducibility. The measurement time of 250 s, in this case, is even more conservative because the steady state is reached just after 50 s. The sensor shows an excellent response of about 62.3 mV pH^{-1}, Figure 5B, in line with the Nernstian ideal response of 59 mV pH^{-1}, with an R^2 of 0.993 and a main standard deviation of 3.8%. We attributed this better behavior of the electrode to the presence of rGO which acts as a protective layer of the ITO substrate, inhibiting its partial dissolution in an acid environment. Therefore, it can be concluded that the rGO/PANI double-layer electrode has the better performance, and thus these types of electrodes were used for the interference tests and for the analyses of real sweat samples.
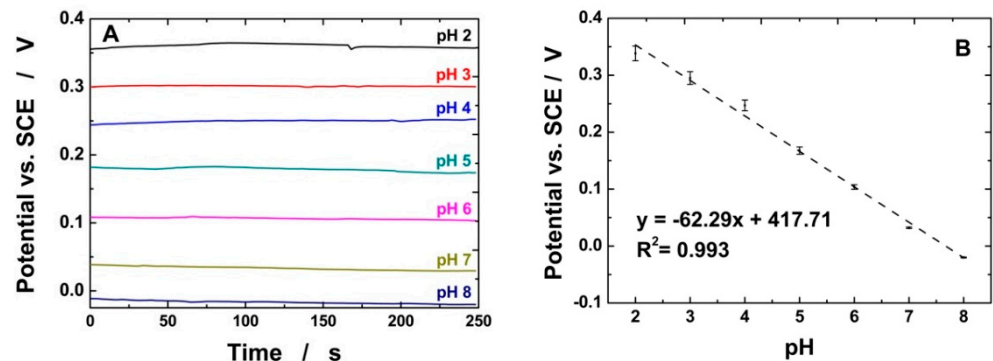

Figure 5. (**A**) OCP vs. time curves; (**B**) calibration line of PANI/rGO/ITO-PET electrode.

In order to verify the selectivity of PANI-rGO-ITO-PET electrodes, the influence of various interfering species present in the matrix of real samples of human sweat was studied. In particular, interferences toward sodium, chloride, ammonia and potassium ions and lactic acid [84,85] were tested. In detail, 25 mM of Na$^+$ and Cl$^-$, 0.45 mM of NH$_4$$^+$, 1.75 mM of K$^+$ and 7.5 mM of lactic acid were injected into a PBS at pH 6. This value was selected because it is the intermediate value of the pH of sweat that can vary from pH 4 to 8 [27]. The concentration of interfering agents was selected in order to simulate the sweat composition. Tests were conducted measuring the OCP for 250 s. The results reported in Figure 6 show that there are negligible interference effects in the pH determination, and the maximum variation values of about 3.22% and 3.1% were recorded for NaCl and NH$_4$Cl. A negligible interference was also found when all interfering species were added together in solution.
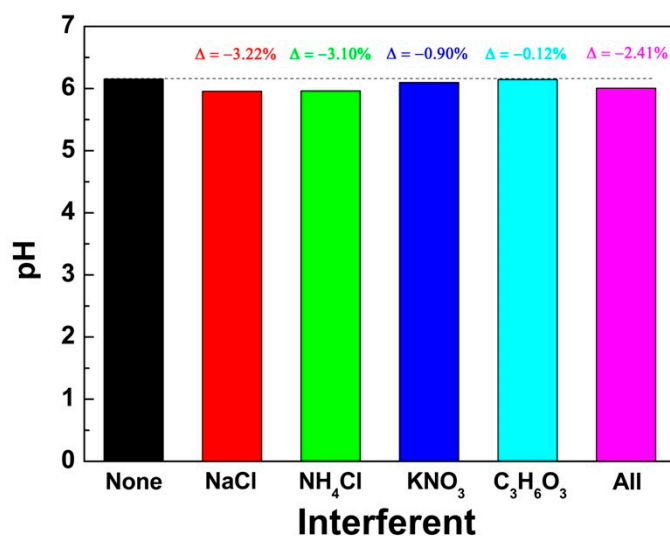
Figure 6. Influence of 25 mM of Na^+ and Cl^-, 0.45 mM of NH_{4+}, 1.75 mM of K^+ and 7.5 mM of lactic acid.

To validate the sensor, a real sweat sample was collected on the forehead of a healthy subject according to the method proposed in [70]. The obtained result was corroborated using a laboratory pH meter. The sweat was analyzed without any treatment. In particular, the same electrode was used to measure the pH in the sweat and four different buffer solutions. As it can be observed in Figure 7, the OCP curve of the sweat is similar to that of the buffer solution. Using the calibration line of Figure 5, a pH sweat value of 4.3 was obtained. This result agrees with the pH value measured with the pH meter, which is 4.4 ± 0.1.
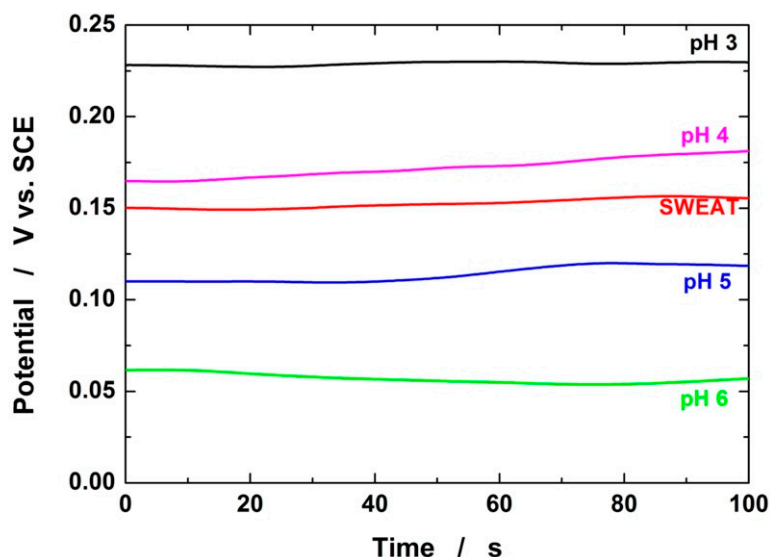

Figure 7. OCP vs. time curves for sweat real sample and for buffer solution at different pH.

In order to compare the performance of our electrodes with the data present in the literature, in Table 1, the main principal parameters of the electrochemical behavior of different pH sensors are reported. As it is shown, the proposed sensor performances are in line with those of the electrodes selected for Table 1. The good performance combined with other advantages (flexibility, short preparation time, simplicity of the electrochemical method, low preparation cost, easily scalability) make this sensor applicable on a large scale.

Table 1. Comparison between pH electrochemical sensors.

	pH Range	Sensitivity	Flexible	Easy Fabrication	Interference	Real Samples	Ref
PI-PANI	5.5–8.5	58.6	Y	N	N.S.	N.S.	[86]
PET-PANI	2–12	60.3	Y	N	Na^+, K^+, NH_4^+, Ca^{2+}, Mg^{2+}	coke, coffee, water, orange juice	[87]
CPE-PANI	3–10	62.4	Y	Y	Ca^{2+}, Mg^{2+}, K^+, Na^+, NH_4^+	milk and apples	[88]
LbL/(PANI-GA/GO)	2–7	35.1	Y	Y	N.S.	N.S.	[89]
NH_2-G/PANI	1–11	50.7	N	Y	N.S.	N.S.	[90]
PANI-NWs-ITO	3–9	48	N	Y	N.S.	N.S.	[91]
PANI-PS	4–8	59	N	Y	N.S.	N.S.	[92]
PANI/PU	2–7	60	Y	Y	N.S.	sweat	[30]
GCE/GMC@PANI	2–11	58	N	Y	$NaCl$, NH_4Cl, KNO_3, AA, UA, GLU, $NaNO_3$, $NaNO_2$, HYD, DA, CYS	urine, saliva	[93]
PANI Cable	4–10	58.7	Y	Y	Na^+, K^+, NH_4^+, Ca^{2+},	urine, sweat, saliva, tears	[94]
Bandage-PANI	5.5–8	58	Y	Y	$NaCl$, KCl, Na_2SO_4	serum, SWS	[95]
IrO_2/G	3–8	79	Y	N	Na+, Cl-, K+, SA	sweat	[28]
ITO-rGO-PANI	2–8	62.3	Y	Y	$NaCl$, NH_4Cl, KNO_3, LA	sweat	ThisWork

ITO: indium tin oxide; rGO: reduced graphene oxide; PANI: polyaniline; LA: lactic acid; PI: polyimide; CPE: carbon paste electrode; LbL: layer by layer; GA: gum arabic; G: graphite; GO: graphene oxide; NWs: nanowires; PS: a polysaccharide; PU: polyurethane; GLU: glucose; HYD: hydraine; DA: dopamine; CYS: cysteine; UA: uric acid; AA: ascorbic acid; GCE: glassy carbon electrode; GMC: graphitized mesoporous carbon; SWS: simulated wound solution; N.S.: not studied.

4. Conclusions

In this work, wearable PANI-based sensors were manufactured for electrochemical pH measurement. As a substrate for PANI electrodeposition, thin and flexible ITO-PET was employed. To obtain the desired oxidation state, the emeraldine form, PANI electrodeposition was carried out by potentiostatic deposition. After manufacturing, ITO-PET/PANI was tested as a pH sensor by measuring the OCP. The results show good reproducibility at a neutral-basic pH but poor reproducibility at a lower pH; moreover, the slope of the calibration line was low and far from the Nernstian values. Then, to improve the performance of the sensor, rGO was added to the substrate prior to PANI deposition. Using the same technique, ITO-PET/rGO/PANI double-layer electrodes showed a high reproducibility in the whole pH scale between 2 and 8, also reporting a slope of 62.29 mV/pH, very close to the Nernst value. In addition, the selectivity of the sensor was investigated using various interferents, chosen from the possible ions and metabolites that can be found in sweat. From the results obtained, it is possible to state that the selectivity in the pH detection of the sensor is very good, with a maximum signal variation of 3.22%. In order to validate the sensor, a real sweat sample was collected from a healthy subject and tested with both the proposed sensor and a commercial pH meter, obtaining a very good concordance. This experiment clearly shows the possibility of using this electrochemical sensor to quantify the pH in real sweat samples.

References

1. Seshadri, D.R.; Li, R.T.; Voos, J.E.; Rowbottom, J.R.; Alfes, C.M.; Zorman, C.A.; Drummond, C.K. Wearable Sensors for Monitoring the Physiological and Biochemical Profile of the Athlete. *NPJ Digit. Med.* **2019**, *2*, 72. [CrossRef]
2. Heikenfeld, J.; Jajack, A.; Rogers, J.; Gutruf, P.; Tian, L.; Pan, T.; Li, R.; Khine, M.; Kim, J.; Wang, J.; et al. Wearable Sensors: Modalities, Challenges, and Prospects. *Lab Chip* **2018**, *18*, 217–248. [CrossRef]
3. Patel, S.; Park, H.; Bonato, P.; Chan, L.; Rodgers, M. A Review of Wearable Sensors and Systems with Application in Rehabilitation. *J. Neuroeng. Rehabil.* **2012**, *9*, 21. [CrossRef]
4. Seshadri, D.R.; Davies, E.V.; Harlow, E.R.; Hsu, J.J.; Knighton, S.C.; Walker, T.A.; Voos, J.E.; Drummond, C.K. Wearable Sensors for COVID-19: A Call to Action to Harness Our Digital Infrastructure for Remote Patient Monitoring and Virtual Assessments. *Front. Digit. Health* **2020**, *2*, 8. [CrossRef]
5. Angelucci, A.; Cavicchioli, M.; Cintorrino, I.A.; Lauricella, G.; Rossi, C.; Strati, S.; Aliverti, A. Smart Textiles and Sensorized Garments for Physiological Monitoring: A Review of Available Solutions and Techniques. *Sensors* **2021**, *21*, 814. [CrossRef] [PubMed]
6. Kim, H.; Kim, S.; Lee, M.; Rhee, Y.; Lee, S.; Jeong, Y.-R.; Kang, S.; Naqi, M.; Hong, S. Smart Patch for Skin Temperature: Preliminary Study to Evaluate Psychometrics and Feasibility. *Sensors* **2021**, *21*, 1855. [CrossRef]
7. Gaubert, V.; Gidik, H.; Koncar, V. Proposal of a Lab Bench for the Unobtrusive Monitoring of the Bladder Fullness with Bioimpedance Measurements. *Sensors* **2020**, *20*, 3980. [CrossRef] [PubMed]
8. Oliveira, A.; Dias, D.; Múrias Lopes, E.; Vilas-Boas, M.d.C.; Paulo Silva Cunha, J. SnapKi—An Inertial Easy-to-Adapt Wearable Textile Device for Movement Quantification of Neurological Patients. *Sensors* **2020**, *20*, 3875. [CrossRef]
9. Pham, S.; Yeap, D.; Escalera, G.; Basu, R.; Wu, X.; Kenyon, N.J.; Hertz-Picciotto, I.; Ko, M.J.; Davis, C.E. Wearable Sensor System to Monitor Physical Activity and the Physiological Effects of Heat Exposure. *Sensors* **2020**, *20*, 855. [CrossRef]
10. Davis-Martin, R.E.; Alessi, S.M.; Boudreaux, E.D. Alcohol Use Disorder in the Age of Technology: A Review of Wearable Biosensors in Alcohol Use Disorder Treatment. *Front. Psychiatry* **2021**, *12*, 642813. [CrossRef]
11. Madden, J.; O'Mahony, C.; Thompson, M.; O'Riordan, A.; Galvin, P. Biosensing in Dermal Interstitial Fluid Using Microneedle Based Electrochemical Devices. *Sens. Bio-Sens. Res.* **2020**, *29*, 100348. [CrossRef]
12. Barrett, C.; O'Sullivan, F.; Barry, S.; Grygoryev, K.; O'Gorman, D.; O'Mahony, C.; O'Riordan, A. Novel Surface Modified Polymer Microneedle Based Biosensors for Interstitial Fluid Glucose Detection. In Proceedings of the 2019 IEEE SENSORS, Montreal, QC, Canada, 27–30 October 2019; pp. 1–4.
13. Park, H.; Park, W.; Lee, C.H. Electrochemically Active Materials and Wearable Biosensors for the in Situ Analysis of Body Fluids for Human Healthcare. *NPG Asia Mater.* **2021**, *13*, 23. [CrossRef]
14. Wang, Z.; Shin, J.; Park, J.; Lee, H.; Kim, D.; Liu, H. Engineering Materials for Electrochemical Sweat Sensing. *Adv. Funct. Mater.* **2021**, *31*, 2008130. [CrossRef]
15. Bondioli, M.; Chessa, S.; Narzisi, A.; Pelagatti, S.; Zoncheddu, M. Towards Motor-Based Early Detection of Autism Red Flags: Enabling Technology and Exploratory Study Protocol. *Sensors* **2021**, *21*, 1971. [CrossRef] [PubMed]
16. Wasiewska, L.A.; Seymour, I.; Patella, B.; Inguanta, R.; Burgess, C.M.; Duffy, G.; O'Riordan, A. Reagent Free Electrochemical-Based Detection of Silver Ions at Interdigitated Microelectrodes Using in-Situ PH Control. *Sens. Actuators B Chem.* **2021**, 129531. [CrossRef]

17. Seymour, I.; O'Sullivan, B.; Lovera, P.; Rohan, J.F.; O'Riordan, A. Electrochemical Detection of Free-Chlorine in Water Samples Facilitated by in-Situ PH Control Using Interdigitated Microelectrodes. *Sens. Actuators B Chem.* **2020**, *325*, 128774. [CrossRef]
18. Wahl, A.J.C.; Seymour, I.P.; Moore, M.; Lovera, P.; O'Riordan, A.; Rohan, J.F. Diffusion Profile Simulations and Enhanced Iron Sensing in Generator-Collector Mode at Interdigitated Nanowire Electrode Arrays. *Electrochim. Acta* **2018**, *277*, 235–243. [CrossRef]
19. Chen, Y.-L.; Kuan, W.-H.; Liu, C.-L. Comparative Study of the Composition of Sweat from Eccrine and Apocrine Sweat Glands during Exercise and in Heat. *IJERPH* **2020**, *17*, 3377. [CrossRef]
20. Gonçalves, A.C.; Marson, F.A.L.; Mendonça, R.M.H.; Bertuzzo, C.S.; Paschoal, I.A.; Ribeiro, J.D.; Ribeiro, A.F.; Levy, C.E. Chloride and Sodium Ion Concentrations in Saliva and Sweat as a Method to Diagnose Cystic Fibrosis. *J. Pediatr.* **2019**, *95*, 443–450. [CrossRef]
21. Liamis, G. Diabetes Mellitus and Electrolyte Disorders. *WJCC* **2014**, *2*, 488. [CrossRef]
22. Pascual, E.; Addadi, L.; Andrés, M.; Sivera, F. Mechanisms of Crystal Formation in Gout—A Structural Approach. *Nat. Rev. Rheumatol.* **2015**, *11*, 725–730. [CrossRef] [PubMed]
23. Worthley, L.I.G. Hydrogen Ion Metabolism. *Anaesth Intensive Care* **1977**, *5*, 347–360. [CrossRef] [PubMed]
24. Daudon, M.; Traxer, O.; Conort, P.; Lacour, B.; Jungers, P. Type 2 Diabetes Increases the Risk for Uric Acid Stones. *JASN* **2006**, *17*, 2026–2033. [CrossRef]
25. Schmid-Wendtner, M.-H.; Korting, H.C. The PH of the Skin Surface and Its Impact on the Barrier Function. *Skin Pharmacol. Physiol.* **2006**, *19*, 296–302. [CrossRef] [PubMed]
26. Possanzini, L.; Decataldo, F.; Mariani, F.; Gualandi, I.; Tessarolo, M.; Scavetta, E.; Fraboni, B. Textile Sensors Platform for the Selective and Simultaneous Detection of Chloride Ion and PH in Sweat. *Sci. Rep.* **2020**, *10*, 17180. [CrossRef] [PubMed]
27. Coyle, S.; Morris, D.; Lau, K.-T.; Diamond, D.; Taccini, N. Textile Sensors to Measure Sweat PH and Sweat-Rate during Exercise. In Proceedings of the 2009 3rd International Conference on Pervasive Computing Technologies for Healthcare, London, UK, 1–3 April 2009.
28. Mazzaracchio, V.; Fiore, L.; Nappi, S.; Marrocco, G.; Arduini, F. Medium-Distance Affordable, Flexible and Wireless Epidermal Sensor for PH Monitoring in Sweat. *Talanta* **2021**, *222*, 121502. [CrossRef] [PubMed]
29. Vinoth, R.; Nakagawa, T.; Mathiyarasu, J.; Mohan, A.M.V. Fully Printed Wearable Microfluidic Devices for High-Throughput Sweat Sampling and Multiplexed Electrochemical Analysis. *ACS Sens.* **2021**, *6*, 1174–1186. [CrossRef] [PubMed]
30. Hou, X.; Zhou, Y.; Liu, Y.; Wang, L.; Wang, J. Coaxial Electrospun Flexible PANI//PU Fibers as Highly Sensitive PH Wearable Sensor. *J. Mater. Sci.* **2020**, *55*, 16033–16047. [CrossRef]
31. Wang, R.; Zhai, Q.; Zhao, Y.; An, T.; Gong, S.; Guo, Z.; Shi, Q.; Yong, Z.; Cheng, W. Stretchable Gold Fiber-Based Wearable Electrochemical Sensor toward PH Monitoring. *J. Mater. Chem. B* **2020**, *8*, 3655–3660. [CrossRef] [PubMed]
32. Diculescu, V.C.; Beregoi, M.; Evanghelidis, A.; Negrea, R.F.; Apostol, N.G.; Enculescu, I. Palladium/Palladium Oxide Coated Electrospun Fibers for Wearable Sweat PH-Sensors. *Sci. Rep.* **2019**, *9*, 8902. [CrossRef] [PubMed]
33. Manjakkal, L.; Dang, W.; Yogeswaran, N.; Dahiya, R. Textile-Based Potentiometric Electrochemical PH Sensor for Wearable Applications. *Biosensors* **2019**, *9*, 14. [CrossRef] [PubMed]
34. Dang, W.; Manjakkal, L.; Navaraj, W.T.; Lorenzelli, L.; Vinciguerra, V.; Dahiya, R. Stretchable Wireless System for Sweat PH Monitoring. *Biosens. Bioelectron.* **2018**, *107*, 192–202. [CrossRef]
35. Wang, H.; Lin, J.; Shen, Z.X. Polyaniline (PANi) Based Electrode Materials for Energy Storage and Conversion. *J. Sci. Adv. Mater. Devices* **2016**, *1*, 225–255. [CrossRef]
36. Hatchett, D.W.; Josowicz, M.; Janata, J. Acid Doping of Polyaniline: Spectroscopic and Electrochemical Studies. *J. Phys. Chem. B* **1999**, *103*, 10992–10998. [CrossRef]
37. Zare, E.N.; Makvandi, P.; Ashtari, B.; Rossi, F.; Motahari, A.; Perale, G. Progress in Conductive Polyaniline-Based Nanocomposites for Biomedical Applications: A Review. *J. Med. Chem.* **2020**, *63*, 1–22. [CrossRef]
38. Gvozdenovic, M.; Jugovic, B.; Stevanovic, J.; Grgur, B. Electrochemical Synthesis of Electroconducting Polymers. *Hem Ind* **2014**, *68*, 673–684. [CrossRef]
39. Kobayashi, T.; Yoneyama, H.; Tamura, H. Electrochemical Reactions Concerned with Electrochromism of Polyaniline Film-Coated Electrodes. *J. Electroanal. Chem. Interfacial Electrochem.* **1984**, *177*, 281–291. [CrossRef]
40. Lindfors, T.; Ervelä, S.; Ivaska, A. Polyaniline as PH-Sensitive Component in Plasticized PVC Membranes. *J. Electroanal. Chem.* **2003**, *560*, 69–78. [CrossRef]
41. Dispenza, C.; Sabatino, M.A.; Deghiedy, N.; Casaletto, M.P.; Spadaro, G.; Piazza, S.; Abd El-Rehim, H.A. In-Situ Polymerization of Polyaniline in Radiation Functionalized Polypropylene Films. *Polymer* **2015**, *67*, 128–138. [CrossRef]
42. Dispenza, C.; Fiandaca, G.; Lo Presti, C.; Piazza, S.; Spadaro, G. Electrical Properties of γ-Crosslinked Hydrogels Incorporating Organic Conducting Polymers. *Radiat. Phys. Chem.* **2007**, *76*, 1371–1375. [CrossRef]
43. Brochocka, A.; Nowak, A.; Zajączkowska, H.; Sieradzka, M. Chemosensitive Thin Films Active to Ammonia Vapours. *Sensors* **2021**, *21*, 2948. [CrossRef] [PubMed]
44. Kim, J.Y.; Iqbal, S.; Jang, H.J.; Jung, E.Y.; Bae, G.T.; Park, C.S.; Shin, B.J.; Tae, H.S. Transparent Polyaniline Thin Film Synthesized Using a Low-Voltage-Driven Atmospheric Pressure Plasma Reactor. *Materials* **2021**, *14*, 1278. [CrossRef] [PubMed]
45. Zhong, F.; Ma, M.; Zhong, Z.; Lin, X.; Chen, M. Interfacial Growth of Free-Standing PANI Films: Toward High-Performance All-Polymer Supercapacitors. *Chem. Sci.* **2021**, *12*, 1783–1790. [CrossRef]

46. Medi, B.; Bahramian, A.; Nazari, V. Synthesis and Characterization of Conducting Polyaniline Nanostructured Thin Films for Solar Cell Applications. *JOM* **2021**, *73*, 504–514. [CrossRef]

47. Akber, H.J.; Ibrahim, I.M.; Razeg, K.H. Hydrothermal Synthesis of Polyaniline Nano-Fibers as H_2S Gas Sensor. *J. Phys. Conf. Ser.* **2020**, *1664*, 012017. [CrossRef]

48. Demuru, S.; Kunnel, B.P.; Briand, D. Thin Film Organic Electrochemical Transistors Based on Hybrid PANI/PEDOT:PSS Active Layers for Enhanced PH Sensing. *Biosens. Bioelectron. X* **2021**, *7*, 100065. [CrossRef]

49. Silipigni, L.; Barreca, F.; Fazio, E.; Neri, F.; Spanò, T.; Piazza, S.; Sunseri, C.; Inguanta, R. Template Electrochemical Growth and Properties of Mo Oxide Nanostructures. *J. Phys. Chem. C* **2014**, *118*, 22299–22308. [CrossRef]

50. Battaglia, M.; Piazza, S.; Sunseri, C.; Inguanta, R. Amorphous Silicon Nanotubes via Galvanic Displacement Deposition. *Electrochem. Commun.* **2013**, *34*, 134–137. [CrossRef]

51. Battaglia, M.; Inguanta, R.; Piazza, S.; Sunseri, C. Fabrication and Characterization of Nanostructured Ni–IrO2 Electrodes for Water Electrolysis. *Int. J. Hydrog. Energy* **2014**, *39*, 16797–16805. [CrossRef]

52. Ganci, F.; Lombardo, S.; Sunseri, C.; Inguanta, R. Nanostructured Electrodes for Hydrogen Production in Alkaline Electrolyzer. *Renew. Energy* **2018**, *123*, 117–124. [CrossRef]

53. Patella, B.; Piazza, S.; Sunseri, C.; Inguanta, R. Nio Thin Film for Mercury Detection in Water by Square Wave Anodic Stripping Voltammetry. *Chem. Eng. Trans.* **2017**, *60*, 1–6. [CrossRef]

54. Insinga, M.G.; Oliveri, R.L.; Sunseri, C.; Inguanta, R. Template Electrodeposition and Characterization of Nanostructured Pb as a Negative Electrode for Lead-Acid Battery. *J. Power Sources* **2019**, *413*, 107–116. [CrossRef]

55. Sunseri, C.; Cocchiara, C.; Ganci, F.; Moncada, A.; Oliveri, R.L.; Patella, B.; Piazza, S.; Inguanta, R. Nanostructured Electrochemical Devices for Sensing, Energy Conversion and Storage. *Chem. Eng. Trans.* **2016**, *47*, 43–48. [CrossRef]

56. Patella, B.; Buscetta, M.; Di Vincenzo, S.; Ferraro, M.; Aiello, G.; Sunseri, C.; Pace, E.; Inguanta, R.; Cipollina, C. Electrochemical Sensor Based on RGO/Au Nanoparticles for Monitoring H2O2 Released by Human Macrophages. *Sens. Actuators B Chem.* **2021**, *327*, 128901. [CrossRef]

57. Patella, B.; Russo, R.R.; O'Riordan, A.; Aiello, G.; Sunseri, C.; Inguanta, R. Copper Nanowire Array as Highly Selective Electrochemical Sensor of Nitrate Ions in Water. *Talanta* **2021**, *221*, 121643. [CrossRef]

58. Belgherbi, O.; Seid, L.; Lakhdari, D.; Chouder, D.; Akhtar, M.S.; Saeed, M.A. Optical and Morphological Properties of Electropolymerized Semiconductor Polyaniline Thin Films: Effect of Thickness. *J. Electron. Mater.* **2021**, *50*, 3876–3884. [CrossRef]

59. Nekrasov, A.A.; Iakobson, O.D.; Gribkova, O.L.; Pozin, S.I. Raman Spectroelectrochemical Monitoring of Conducting Polymer Electrosynthesis on Reflective Metallic Electrode: Effects Due to Double Excitation of the Electrode/Film/Solution Interfaces. *J. Electroanal. Chem.* **2020**, *873*, 114415. [CrossRef]

60. Palma-Cando, A.; Rendón-Enríquez, I.; Tausch, M.; Scherf, U. Thin Functional Polymer Films by Electropolymerization. *Nanomaterials* **2019**, *9*, 1125. [CrossRef] [PubMed]

61. Quijada, C.; Leite-Rosa, L.; Berenguer, R.; Bou-Belda, E. Enhanced Adsorptive Properties and Pseudocapacitance of Flexible Polyaniline-Activated Carbon Cloth Composites Synthesized Electrochemically in a Filter-Press Cell. *Materials* **2019**, *12*, 2516. [CrossRef] [PubMed]

62. Mazzara, F.; Patella, B.; Aiello, G.; O'Riordan, A.; Torino, C.; Vilasi, A.; Inguanta, R. Electrochemical Detection of Uric Acid and Ascorbic Acid Using R-GO/NPs Based Sensors. *Electrochim. Acta* **2021**, *388*, 138652. [CrossRef]

63. Li, S.; Ma, Y.; Liu, Y.; Xin, G.; Wang, M.; Zhang, Z.; Liu, Z. Electrochemical Sensor Based on a Three Dimensional Nanostructured MoS_2 Nanosphere-PANI/Reduced Graphene Oxide Composite for Simultaneous Detection of Ascorbic Acid, Dopamine, and Uric Acid. *RSC Adv.* **2019**, *9*, 2997–3003. [CrossRef]

64. Anand, V.K.; Bukke, A.; Bhatt, K.; Kumar, S.; Sharma, S.; Goyal, R.; Virdi, G.S. Highly Sensitive and Reusable Cu+2/Polyaniline/ Reduced Graphene Oxide Nanocomposite Ink-Based Non-Enzymatic Glucose Sensor. *Appl. Phys. A* **2020**, *126*, 500. [CrossRef]

65. Du, X.; Chen, Y.; Dong, W.; Han, B.; Liu, M.; Chen, Q.; Zhou, J. A Nanocomposite-Based Electrochemical Sensor for Non-Enzymatic Detection of Hydrogen Peroxide. *Oncotarget* **2017**, *8*, 13039–13047. [CrossRef]

66. Aryal, K.P.; Jeong, H.K. Simultaneous Determination of Ascorbic Acid, Dopamine, and Uric Acid with Polyaniline/Hemin/Reduced Graphite Oxide Composite. *Chem. Phys. Lett.* **2021**, *768*, 138405. [CrossRef]

67. Xue, C.; Wang, X.; Zhu, W.; Han, Q.; Zhu, C.; Hong, J.; Zhou, X.; Jiang, H. Electrochemical Serotonin Sensing Interface Based on Double-Layered Membrane of Reduced Graphene Oxide/Polyaniline Nanocomposites and Molecularly Imprinted Polymers Embedded with Gold Nanoparticles. *Sens. Actuators B Chem.* **2014**, *196*, 57–63. [CrossRef]

68. Wirth, D.M.; Waldman, L.J.; Petty, M.; LeBlanc, G. Communication—Polyaniline Electrodeposition on Flexible ITO Substrates and the Effect of Curved Electrochemical Conditions. *J. Electrochem. Soc.* **2019**, *166*, D635–D637. [CrossRef]

69. Zhu, C.; Guo, S.; Fang, Y.; Han, L.; Wang, E.; Dong, S. One-Step Electrochemical Approach to the Synthesis of Graphene/MnO2 Nanowall Hybrids. *Nano Res.* **2011**, *4*, 648–657. [CrossRef]

70. Erez, M.; Zaykovsky, Z. Sweat Collectors and Methods of Collecting Sweat. U.S. Patent 8,215,192, 10 July 2012.

71. Inguanta, R.; Garlisi, C.; Spanò, T.; Piazza, S.; Sunseri, C. Growth and Photoelectrochemical Behaviour of Electrodeposited ZnO Thin Films for Solar Cells. *J. Appl. Electrochem.* **2013**, *43*, 199–208. [CrossRef]

72. Butoi, B.; Groza, A.; Dinca, P.; Balan, A.; Barna, V. Morphological and Structural Analysis of Polyaniline and Poly(o-Anisidine) Layers Generated in a DC Glow Discharge Plasma by Using an Oblique Angle Electrode Deposition Configuration. *Polymers* **2017**, *9*, 732. [CrossRef] [PubMed]

73. Freitas, T.V.; Sousa, E.A.; Fuzari Jr, G.C.; Arlindo, E.P.S. Different Morphologies of Polyaniline Nanostructures Synthesized by Interfacial Polymerization. *Mater. Lett.* **2018**, *224*, 42–45. [CrossRef]

74. Komathi, S.; Gopalan, A.I.; Muthuchamy, N.; Lee, K.P. Polyaniline Nanoflowers Grafted onto Nanodiamonds via a Soft Template-Guided Secondary Nucleation Process for High-Performance Glucose Sensing. *RSC Adv.* **2017**, *7*, 15342–15351. [CrossRef]

75. Patella, B.; Sortino, A.; Aiello, G.; Sunseri, C.; Inguanta, R. Reduced Graphene Oxide Decorated with Metals Nanoparticles Electrode as Electrochemical Sensor for Dopamine. In Proceedings of the 2019 IEEE International Conference on Flexible and Printable Sensors and Systems (FLEPS), Glasgow, UK, 8–10 July 2019; pp. 1–3.

76. Mazzara, F.; Patella, B.; Aiello, G.; Sunseri, C.; Inguanta, R. Ascorbic Acid Determination Using Linear Sweep Voltammetry on Flexible Electrode Modified with Gold Nanoparticles and Reduced Graphene Oxide. In Proceedings of the 2020 IEEE 20th Mediterranean Electrotechnical Conference (MELECON), Palermo, Italy, 16–18 June 2020; pp. 406–410.

77. Tran, H.D.; D'Arcy, J.M.; Wang, Y.; Beltramo, P.J.; Strong, V.A.; Kaner, R.B. The Oxidation of Aniline to Produce "Polyaniline": A Process Yielding Many Different Nanoscale Structures. *J. Mater. Chem.* **2011**, *21*, 3534–3550. [CrossRef]

78. Strankowski, M.; Włodarczyk, D.; Piszczyk, Ł.; Strankowska, J. Polyurethane Nanocomposites Containing Reduced Graphene Oxide, FTIR, Raman, and XRD Studies. *J. Spectrosc.* **2016**, *2016*, 7520741. [CrossRef]

79. Trchová, M.; Šeděnková, I.; Tobolková, E.; Stejskal, J. FTIR Spectroscopic and Conductivity Study of the Thermal Degradation of Polyaniline Films. *Polymer Degrad. Stab.* **2004**, *86*, 179–185. [CrossRef]

80. Mitra, M.; Kulsi, C.; Chatterjee, K.; Kargupta, K.; Ganguly, S.; Banerjee, D.; Goswami, S. Reduced Graphene Oxide-Polyaniline Composites—Synthesis, Characterization and Optimization for Thermoelectric Applications. *RSC Adv.* **2015**, *5*, 31039–31048. [CrossRef]

81. Xiong, S.; Wang, Y.; Chu, J.; Wang, X.; Zhang, R.; Gong, M.; Wu, B.; Li, Z. One-Pot Hydrothermal Synthesis of Polyaniline Nanofibers/Reduced Graphene Oxide Nanocomposites and Their Supercapacitive Properties. *High Perform. Polym.* **2019**, *31*, 1238–1247. [CrossRef]

82. Blinova, N.V.; Stejskal, J.; Trchová, M.; Prokeš, J. Control of Polyaniline Conductivity and Contact Angles by Partial Protonation. *Polym. Int.* **2008**, *57*, 66–69. [CrossRef]

83. Akin, I.; Zor, E.; Bingol, H.; Ersoz, M. Green Synthesis of Reduced Graphene Oxide/Polyaniline Composite and Its Application for Salt Rejection by Polysulfone-Based Composite Membranes. *J. Phys. Chem. B* **2014**, *118*, 5707–5716. [CrossRef]

84. Patterson, M.J.; Galloway, S.D.R.; Nimmo, M.A. Variations in Regional Sweat Composition in Normal Human Males. *Exp. Physiol.* **2000**, *85*, 869–875. [CrossRef]

85. Baker, L.B. Physiology of Sweat Gland Function: The Roles of Sweating and Sweat Composition in Human Health. *Temperature* **2019**, *6*, 211–259. [CrossRef] [PubMed]

86. Li, Y.; Mao, Y.; Xiao, C.; Xu, X.; Li, X. Flexible PH Sensor Based on a Conductive PANI Membrane for PH Monitoring. *RSC Adv.* **2020**, *10*, 21–28. [CrossRef]

87. Yoon, J.H.; Hong, S.B.; Yun, S.-O.; Lee, S.J.; Lee, T.J.; Lee, K.G.; Choi, B.G. High Performance Flexible PH Sensor Based on Polyaniline Nanopillar Array Electrode. *J. Colloid Interface Sci.* **2017**, *490*, 53–58. [CrossRef] [PubMed]

88. Park, H.J.; Yoon, J.H.; Lee, K.G.; Choi, B.G. Potentiometric Performance of Flexible PH Sensor Based on Polyaniline Nanofiber Arrays. *Nano Converg.* **2019**, *6*, 9. [CrossRef]

89. Oliveira, R.D.; Pscheidt, J.; Santos, C.S.; Ferreira, R.T.; Marciniuk, G.; Garcia, J.R.; Vidotti, M.; Marchesi, L.F.; Pessoa, C.A. Electrochemical Performance of PH Sensor Based on LbL Films of Polyaniline-Gum Arabic Nanocomposite and Graphene Oxide. *J. Electrochem. Soc.* **2020**, *167*, 047505. [CrossRef]

90. Su, W.; Xu, J.; Ding, X. An Electrochemical PH Sensor Based on the Amino-Functionalized Graphene and Polyaniline Composite Film. *IEEE Trans. Nanobioscience* **2016**, *15*, 812–819. [CrossRef]

91. Ge, C.; Orosz, K.S.; Armstrong, N.R.; Saavedra, S.S. Poly(Aniline) Nanowires in SolÀGel Coated ITO: A PH-Responsive Substrate for Planar Supported Lipid Bilayers. *ACS Appl. Mater. Interfaces* **2011**, *9*, 2677–2685. [CrossRef]

92. Lakard, B. Optimization of the Structural Parameters of New Potentiometric PH and Urea Sensors Based on Polyaniline and a Polysaccharide Coupling Layer. *Sens. Actuators B Chem.* **2012**, *8*, 794–801. [CrossRef]

93. Saikrithika, S. A Selective Voltammetric PH Sensor Using Graphitized Mesoporous Carbon/Polyaniline Hybrid System. *J. Chem. Sci.* **2021**, *10*, 46. [CrossRef]

94. Yoon, J.H. Highly Self-Healable and Flexible Cable-Type PH Sensors for Real-Time Monitoring of Human Fluids. *Biosens. Bioelectron.* **2020**, *7*, 111946. [CrossRef]

95. Guinovart, T.; ValdØs-Ramírez, G.; Windmiller, J.R.; Andrade, F.J.; Wang, J. Bandage-Based Wearable Potentiometric Sensor for Monitoring Wound PH. *Electroanalysis* **2014**, *9*, 1345–1353. [CrossRef]